ACS OMEGA

http://pubs.acs.org/journal/acsodf

Article

# Solvent Evaporation Induced Large-Scale Synthesis of $Cs_4PbBr_6$ and $CsPbBr_3$ Microcrystals: Optical Properties and Backlight Application for LEDs

Swapnika Suresh, Mohan Raj Subramaniam, Sobhan Hazra, Bhola Nath Pal, and Sudip K. Batabyal*

Cite This: *ACS Omega* 2023, 8, 4616−4626

Read Online

ACCESS | Metrics & More | Article Recommendations | Supporting Information

**ABSTRACT:** The contemporary work focuses on embossing the emissive nature of lead halide perovskite materials, specifically $Cs_4PbBr_6$ microcrystal powder prepared via single step bulk recrystallization method followed by the solvent evaporation route from gram to kilogram scale. The X-ray diffraction pattern confirms the formation of phase pure $Cs_4PbBr_6$ with a goodness of fit value of 1.51 calculated from Rietveld refinement and the fluorophore powder manifesting an intrinsic band gap of 3.76 eV. The experimental yield of 99.4% indicates the absence of any unreacted precursors. The fabricated flexible, free-standing $Cs_4PbBr_6$@PMMA film encompassed better moisture stability without undergoing phase transitions for 400 days. The temperature-dependent photoluminescence spectra denote that 51% of the intensity was retained when cooled back to room temperature after heating it till 180 °C. Moisture studies at two extreme humidity conditions also reveal the appreciable stability of the fluorophore film against moisture. The stability studies with respect to UV irradiation substantiate that the film retained its stability even after exposing it continuously to UV radiation for seven days. The outstanding optical properties of these microcrystals, owing to the higher exciton binding energy, make them a promising candidate as excellent fluorophores for color conversion, backlight, and light-emitting applications. The $Cs_4PbBr_6$@PMMA film was employed as the top cover of a commercial blue LED, producing a robust green emission which revealed its possible application as a phosphor material.

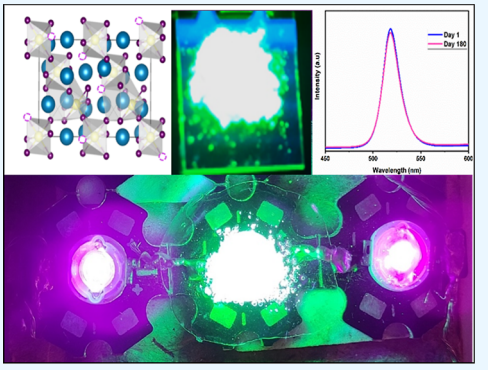


## 1. INTRODUCTION

The magnificent optical properties—essentially, long carrier diffusion length, tunable band gap, defect tolerance capability, high quantum yield, efficient photoluminescence (PL), and tunable emission over a broad spectrum of all cesium lead halide perovskites have marked its applicability and pertinence in optoelectronic applications, for instance, light emitting diodes (LEDs), solar cells, photodetectors, color converters lasers, and others.[1−6] The general formula for perovskites can be depicted as $ABX_3$, where A is a monovalent cation such as $Cs^+$, $CH_3NH_3^+$, B is any divalent metal, normally $Pb^{2+}$, $Sb^{2+}$, $Sn^{2+}$, and X is a halogen anion (X = Cl, Br, I).[2−4] All cesium lead bromide perovskites have acquired considerable attention all over owing to their aforementioned properties and facile synthesis procedure.[3] Based on how the $[PbX_6]^{4-}$ [X = Cl, Br, I] octahedra are connected, they can form different structures including corner shared octahedra (for 3D), layered networks (2D), long chains(1D), and isolated dots (0D).[1,2] It is well evident that each of these crystalline structures exhibits versatile physical and chemical properties.[6]

Also, the ratio of precursors plays a major role in the stoichiometry of the so-formed perovskite solids. Mixing distinct ratios of CsBr and $PbBr_2$ into suitable solvents leads to the formation of perovskites of different dimensionalities.[7,8] Stringently, fruitful research is going on the synthesis of 0D $Cs_4Pbr_6$, 3D $CsPbBr_3$, and their composites[9] owing to their excellent luminescent properties though the origin behind the luminescent mechanism is still uncertain.[10] Most of the optoelectronic applications including solar cells and LEDs are focused on developing microcrystals with fewer defects so that the recombination of charge carriers is reduced and is more stable when compared to nanocrystals. Hence, micro-sized crystals with fewer defects are high on demand for optoelectronic devices. Among the many, 0D $Cs_4PbBr_6$ with robust green emission has pivoted the research interest into these areas of intervention involving the manufacturing of optoelectronic devices together with LEDs. A good deal of strategies including antisolvent vapor assisted crystallization,[11,12] inverse temperature crystallization, anion−cation reactions[13] ligand assisted super saturated recrystallization,[7] inhomogeneous interface reaction routes,[14] reverse micro-

Received: September 9, 2022
Accepted: December 27, 2022
Published: January 28, 2023

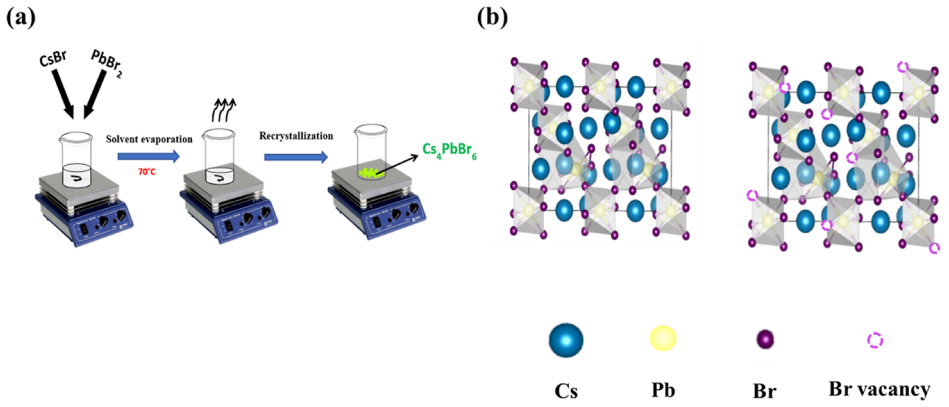


**Figure 1.** (a) Schematic for the synthesis of $Cs_4PbBr_6$ microcrystals (b) Simulated crystal structure of trigonal $Cs_4PbBr_6$ without and with bromine (Br) vacancies, respectively.

emulsion techniques,[15] and Couette−Taylor flow method[2,16] have been explored for the synthesis of $Cs_4PbBr_6$ perovskite solids. Bakr et al. reported the synthesis of pure phase perovskite solids via low-cost and low-temperature solution processing methods.[3,17] But all these methodologies either demand the presence of ligands (dodecylamine, oleylamine, oleic acid, etc.), a suitable solvent [dimethyl sulfoxide (DMSO), *N*,*N*-dimethylformamide (DMF), etc.], or anti-solvent pairs (toluene, dichloromethane, *n*-hexane, etc.) or involves complex procedures.[17] Also, most of the synthesis methods are focused on developing fluorescent perovskite quantum dots[18] rather than in the bulk perovskite microcrystal form which is non-fluorescent in most cases.[19,20] Though perovskite quantum dots are highly luminescent in nature, the stability of these structures is often threatened due to their hydrophobicity, fragility against moisture, and easily strayed halide atoms.[6] Encapsulating perovskite solids with polymer matrices,[21] various inorganic salts,[22] zeolite-Y,[10] and forming core−shell structures are efficient ways to enhance water, thermal, and light stability. Qingyun He et al. reported a novel strategy by coating halide perovskites on polyvinyl butyral (PVB) and forming an HPSs@PVB composite membrane which was applied in backlight displays owing to its excellent optical properties, flexibility, high water, and thermal stability.[16] Meanwhile, Naresh et al. integrated the $CsPbX_3$ [X = $(Cl_{0.5}/Br_{0.5})$, Br, and $(Br_{0.4}/I_{0.6})$] PNCs@$SiO_2$/polymethyl methacrylate (PMMA) composite film employed as an efficient color converter from ultraviolet (UV) to visible for white LEDs and backlighting.[23] Needless to say, some inexorable menace is prone to occur all through the synthesis routes aforementioned, especially during large-scale production. Hence, it is high time to look forward to developing a facile, cost-effective, ligand-free, and environment-friendly synthesis strategy for fluorophore perovskite powders that would cater to the stability threats as well.

Perovskites, especially metal halide perovskites are enthusiastically employed in numerous fields such as Flexible-electronics,[24] photodetectors,[25,26] solar cells,[27] lasers,[28] LEDs,[29] and photo catalysis[30] due to their remarkable optoelectronic properties such as high charge carrier mobility, diffusion length, tunable band gap, and ease of synthesis via low temperature solution processing methods.[31,32] Among them, perovskite based light emitting diodes (p-LEDs) have gained much attention as powerful display devices due to their enhanced external quantum efficiency (EQE) from 1% to more than 23% as reported by recent literature.[33] One of the major drawbacks that hinder the upliftment of EQE in perovskites is the non-radiative recombination rates arising from crystal defects.[34] To suppress fast exciton quenching, changes are made by experimenting on the emissive layer by combining perovskites with different band gaps forming a self-organized multiple quantum well structures.[34,35] This enables faster energy transfer and thereby reduces fast exciton quenching. Changing the morphological aspects[31] like developing 3D textured morphologies as well as tuning the dimensionality[36] can also effectively enhance the performance. The stability of perovskites also raises a major concern in the development of p-LEDs. Embedding the perovskite material on polymer matrices[37,38] and coating the top layer with epoxy resins[39] has been carried out during practical applications of p-LEDs to prevent damage to perovskite structure when exposed to water and moisture. The era of flexible electronics unfolds a broad spectrum of applications including wearable electronics, flexible displays,[40−43] and even submissive energy harvesting devices.[44,45] Numerous display technologies have been developed in the field of wearable electronics among which LEDs have taken a major lead as powerful display devices.[46] Research has shown an ardent approach to manufacture scalable electronic devices fabricated directly on flexible substrates. Concurrently, free-standing polymer films have emerged as flexible substrates in applications such as sensing, micromachining, and consumer electronics which are intended to be cost-effective, thin, easily disposable, and resistant to deformation.[43,46] To date, there exist different techniques for creating white light using LEDs including conventional chip-level conversion, usage of mixing chamber and remote optic to integrate a phosphor, quantum dots,[47] perovskites,[33] or any converting materials (dyes and fluorophores) which in turn converts the blue light of a diode into white light.[48] Mixing LEDs of different colors (red, green, and blue) by a method of color mixing is also an efficient way for fabricating white emitting LEDs wherein each LED intensity can be varied accordingly to get a suitable color temperature. But, this method deals with the usage of multiple LEDs leading to high production and manufacturing costs.

Herein, we have established a flexible, free-standing fluorophore film of 0D $Cs_4PbBr_6$ microcrystal powder with excellent stability toward moisture by a single step bulk recrystallization method via solvent evaporation. The yield of the reaction was calculated to be 99.4% indicating no loss of precursors during the reaction. The polymer matrix of PMMA enabled dual protection of $Cs_4PbBr_6$ fluorophore powder from


https://doi.org/10.1021/acsomega.2c05862
ACS Omega 2023, 8, 4616−4626

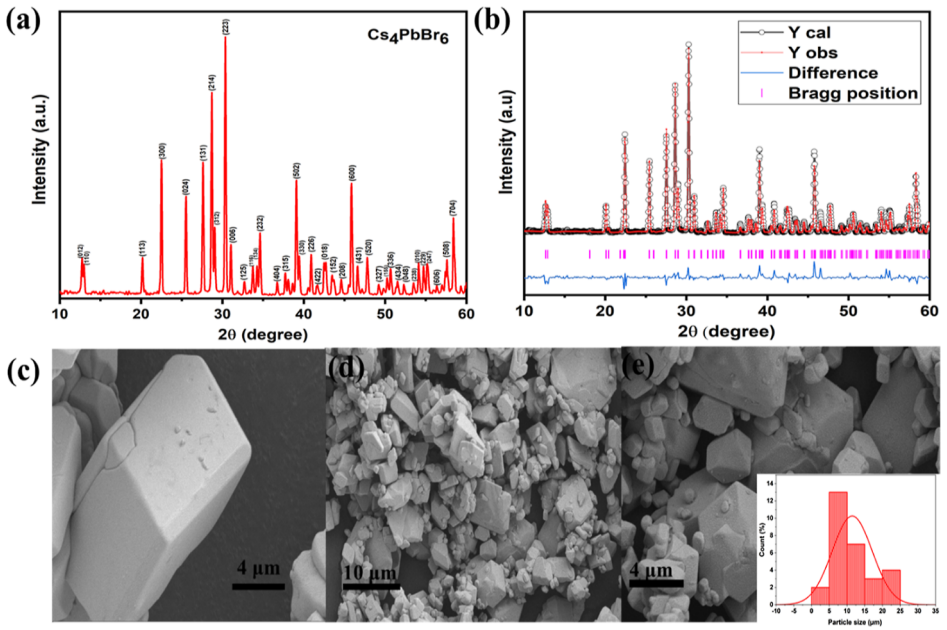


**Figure 2.** XRD patterns of trigonal $Cs_4PbBr_6$ (a) 4:1 concentration of $CsBr/PbBr_2$ (b) after Rietveld Refinement of $Cs_4PbBr_6$. The solid lines and overlying circles show the intensity patterns, calculated and observed, respectively. The pink lines indicate the positions of the calculated Bragg reflections. The blue lines indicate the difference between observed and calculated profiles. (c,d) FE-SEM images of the $Cs_4PbBr_6$ microcrystal at high and low magnification, respectively. (e) SEM image of the $Cs_4PbBr_6$ microcrystal, and the inset figure shows the histogram of particle size.

moisture threats. The as-prepared fluorophore film of $Cs_4PbBr_6$@PMMA exhibits a robust green emission when exposed to UV radiation and pertains its stability for more than 400 days. The fluorophore-PMMA film was found to be stable under different relative humidity (RH) conditions (11 and 84% RH) without undergoing phase transformations or color changes and pertained to be intact even after exposure to UV radiation continuously for 7 days. The free-standing film technique brings forth a compact base for its applications in backlight foundations, color conversion, displays, and light-emitting diodes.

## 2. MATERIALS AND METHODS

**2.1. Materials.** Cesium bromide (CsBr, Sigma-Aldrich, 99.99%), lead(II) bromide ($PbBr_2$, Sigma-Aldrich, 98%), DMF (FINAR, 99.8%), toluene ($C_6H_5CH_3$, Merck, 99.9%), and PMMA (average MW 55,000). All the chemicals and solvents were received and used without further purification.

**2.2. Methods.** *2.2.1. Synthesis of $Cs_4PbBr_6$ Microcrystals.* During the synthesis of $Cs_4PbBr_6$ microcrystals, 0.4 mmol CsBr and 0.1 mmol $PbBr_2$ (4:1 ratio, respectively) were dissolved in 20 mL of DMF, and the solution was stirred at 70 °C for 12 h, as illustrated in Figure 1a. After the reaction period, $Cs_4PbBr_6$ microcrystals were formed in the beaker once the solvent got evaporated completely due to the difference in solubility. The as-synthesized micro-sized crystals were collected and stored for further characterization and analysis. A similar procedure was carried out by altering the precursor concentration to 1:1 ratio for synthesizing bulk $CsPbBr_3$ microcrystals (Supporting Information). The $Cs_4PbBr_6$ microcrystals were embedded in the polymer matrix by manual spreading on the PMMA film at room temperature (Figure S1) for free-standing film fabrication (details of film fabrication explained in Supporting Information).

**2.3. Characterization and Instrumentation.** The X-ray diffraction analysis was performed using an X-ray diffractometer (Rigaku-Ultima 4) using Cu K$\alpha$ radiation ($\lambda$ = 1.54 Å) with a step size of 1°/min. The surface morphology of the samples was characterized using Carl Zeiss, Gemini SEM 300, thermal field emission type scanning electron microscope (FE-SEM). The fluorescence of the samples was analyzed using a U.V. cabinet (model no.: R/340/OB). To understand the emission properties of the fluorophore powder, PL studies were analyzed using PL spectroscopy (RF-6000, Spectrofluorophotometer, Shimadzu). The ultraviolet diffuse reflectance spectroscopic studies (UV-DRS) of the samples were measured by using a Jasco-V-750 spectrophotometer. Intensity analysis of LED outside the $Cs_4PbBr_6$-PMMA coat and LED outside the $Cs_4PbBr_6$ coat was performed using a spectrometer RIFS (RIFS—T1705). The crystal structure of $Cs_4PbBr_6$ was drawn using VESTA software.

**2.4. Calculation of Yield Percentage of $Cs_4PbBr_6$ Microcrystals.**

$$\text{Percentage yield (\%)} = \frac{\text{actual experimental yield}}{\text{theoretical yield}} \times 100\%$$

The theoretical yield was found based on the amount of the limiting reactant ($PbBr_2$) used from the balanced chemical reaction.

$$4CsBr + PbBr_2 \rightarrow Cs_4PbBr_6$$

**2.5. Calculation of Direct Band gap from PL Spectra and from Kubelka Munk Function.** From PL spectra, the direct band gap was calculated using the equation[49]

$$E = \frac{1240}{\lambda}\text{eV} \quad (1)$$

$E$ is the band gap energy in eV, and $\lambda$ is the wavelength in nm.

The direct band gap was also calculated using Kubelka Munk function.[50] The equation for Kubelka Munk is represented as



https://doi.org/10.1021/acsomega.2c05862
ACS Omega 2023, 8, 4616−4626

$$\frac{K}{S} = \frac{(1 - R\infty)}{2\,R\infty} = F_{KM} \quad (2)$$

$R\infty$ is the diffuse reflectance, and $F_{KM}$ is the Kubelka Munk function, $K$ and $S$ are absorption and scattering coefficients, respectively. From this, $(F_{KM} \times h\nu)^{1/n}$ ($n$ = 1/2 for direct band gap materials) were plotted against $h\nu$ for determining the band gap ($E_g$). From the plot of $h\nu$ versus $(F_{KM} \times h\nu)^{1/2}$, the band gap was found from the intersection point between the line extrapolated from the linear region of $(F_{KM} \times h\nu)^{1/2}$ curve and the $h\nu$ axis.

**2.6. Calculation of Efficiency of the $Cs_4PbBr_6$@PMMA Film Using $l_m/W_o$.** Power efficiency of the $Cs_4PbBr_6$@PMMA film was studied with different luminous intensity[51] data. The general equation for conversion of luminous intensity to lumen is given by

$$1 \text{ candela} = 12.57 \text{ lumen}$$

$$l_m/W_o = \frac{\text{lumens} \times \text{spectrometer detector area}}{\text{power density}}$$

## 3. RESULTS AND DISCUSSION

**3.1. Synthesis Scheme and Simulated Structure of $Cs_4PbBr_6$ Microcrystals.** The synthesis of $Cs_4PbBr_6$ microcrystals was carried out via a single step bulk recrystallization method followed by a solvent evaporation route on a laboratory scale. To support the possibility of scaling up the reaction, the yield of the reaction—the theoretical and experimental yield was calculated and was found to be 99.42%. The reason for this higher yield can be attributed to the fact that the precipitate was not washed during the process ensuring no significant loss and arises the possibility of the entire precursor getting converted to perovskite. Moreover, there was no by product or unreacted precursor left after the reaction. Hence, this substantiates the possibility of scaling up the reaction on kilogram scale and there are possibly no limitations for large scale synthesis. Thus, the more the quantity of precursor, the yield will also be proportional since it is a simple evaporation induced method with no loss in the precursor. The X-ray diffraction pattern of the as-prepared perovskite picks out the crystalline structure of 0D $Cs_4PbBr_6$ (Figure 2a). The highly intense peaks imply that the material formed exhibits good crystallinity. The results harmonize well with JCPDS no. 73-2478 and substantiate the formation of the trigonal $Cs_4PbBr_6$ phase in space group $R\bar{3}c$.[2,3] The structural alignment of the lattice follows the Bergerhoff–Schmitz–Dumont-type crystal structure (Figure 1b), wherein the electronic overlap of the adjacent octahedra is minimized by $Cs^+$ ions that result in localized states which are confined to individual octahedra.[46,47] The existence of bromine vacancies (Br) in the $Cs_4PbBr_6$ crystal structure is also depicted in Figure 1b. The presence of this Br vacancy and its influence on the optical properties of the $Cs_4PbBr_6$ microcrystals are discussed in the upcoming session of the manuscript. The crystal structure refinement of the as-prepared $Cs_4PbBr_6$ was carried out by the Rietveld method using the Fullprof Suite software package. The lattice parameters obtained after refinement were found to be in good agreement with the reported data.[9,52] The lattice parameters, weighted profile factor ($R_{wp}$), and expected $R$ factor ($R_{exp}$) is represented in Table 1. The goodness of fit ($G$) was calculated from the ratio of $R_{wp}/R_{exp}$ obtained from the output refined file and was found to be 1.51 (<2) indicating a good Rietveld fit.[53] The Rietveld fit to the well-defined XRD reveals the exclusion of other phases (Figure 2b). The XRD pattern of $Cs_4PbBr_6$@PMMA substantiates that the microcrystals are well embedded in the polymer matrix of PMMA with distinct peaks of $Cs_4PbBr_6$ and PMMA not affecting the lattice of the microcrystals, as shown in Figure S2a. However, the change in the precursor ratio from 4:1 to 1:1 resulted in the formation of mixed monoclinic and orthorhombic phases of 3D $CsPbBr_3$ belonging to space group $P4mm$ (Ref: JCPDS no. 18-0364) and $Pmnb$, (Ref: JCPDS no. 73-2463) [Figure S2b] respectively. The peaks at $2\theta$ = 13.46, 19.13, and 27.31° match well with the JCPDS no. 73-2463 indicating the presence of an orthorhombic phase. There are some unindexed peaks present in the XRD pattern which is also not reported in the literature[54] as well as JCPDS no. 18-0364 at $2\theta$ = 24.16, 25.20, and 28.58° (indexed using asterisk symbol). Hence, the role of the precursor ratio is critical in determining the structure and composition of the material.

**Table 1. Lattice Parameters, $R_{wp}$, $R_{exp}$, and Goodness of Fit ($G$) are Given Below**

| sample | $a$/Å | $b$/Å | $c$/Å | $R_{wp}$/% | $R_{exp}$/% | $G$ |
|---|---|---|---|---|---|---|
| $Cs_4PbBr_6$ | 13.725 | 13.725 | 17.323 | 17.2 | 11.33 | 1.51 |

**3.2. Structural and Morphological Studies.** To further elucidate the microstructure and surface morphologies of the as-synthesized microcrystals, FE-SEM images were taken and are shown in Figure 2c,d (high and low magnification, respectively). The micrographs depict the genesis of particles of micrometer size (~5–25 $\mu$m) with a regular cuboidal-like morphology of $Cs_4PbBr_6$ microcrystals turning into distinct shapes confirming that the formed perovskites can be contemplated as bulk microcrystals. The images reveal the cuboidal morphology of microcrystal powder with longer sides of (16–18 $\mu$m) and shorter sides of (14–16 $\mu$m) (Figure 2c). A histogram of size distribution from SEM (Figure 2e inset) showed that the average particle size was found to be 11.45 $\mu$m. Furthermore, the elemental composition of the microcrystals was analyzed by energy dispersive X-ray spectroscopy (EDX) (Figure S3), and the homogenous distribution of its constituent elements (Figure S4) such as cesium (Cs), lead (Pb), and bromine (Br) by EDX elemental mapping. The stoichiometric ratio of the as-synthesized fluorophore powder symbolizes the phase purity (Table S1). [The micrographs of $CsPbBr_3$ powder are given in Figure S2c].

**3.3. Optical and Emissive Properties of $Cs_4PbBr_6$ Microcrystal Powder.** To analyze the optical performance of the powders, PL and UV-DRS measurements were carried out. Figure 3a represents the green $Cs_4PbBr_6$ microcrystal powder under the ambient light condition that looks extremely different from the orange-colored crystals of $CsPbBr_3$. While illuminating under 365 nm UV light, the green powder exhibits a bright green emission and ultimately no emission for $CsPbBr_3$ (Figure 3b) which indicates that the $Cs_4PbBr_6$ microcrystal powder exhibit magnificent PL performance. The PL spectra of the as-prepared $Cs_4PbBr_6$ powder were found to be a single peak centered at 519 nm (Figure 3c) which is consistent with the reported literature[3] with a FWHM of 22 ± 0.1082 nm. The intense PL emission is owed to the higher exciton binding energy for 0D perovskites of the order of 353 ± 40 meV causing increased radiative recombination rates that dominates over non-radiative deactivation.[3,5,55]



https://doi.org/10.1021/acsomega.2c05862
ACS Omega 2023, 8, 4616–4626

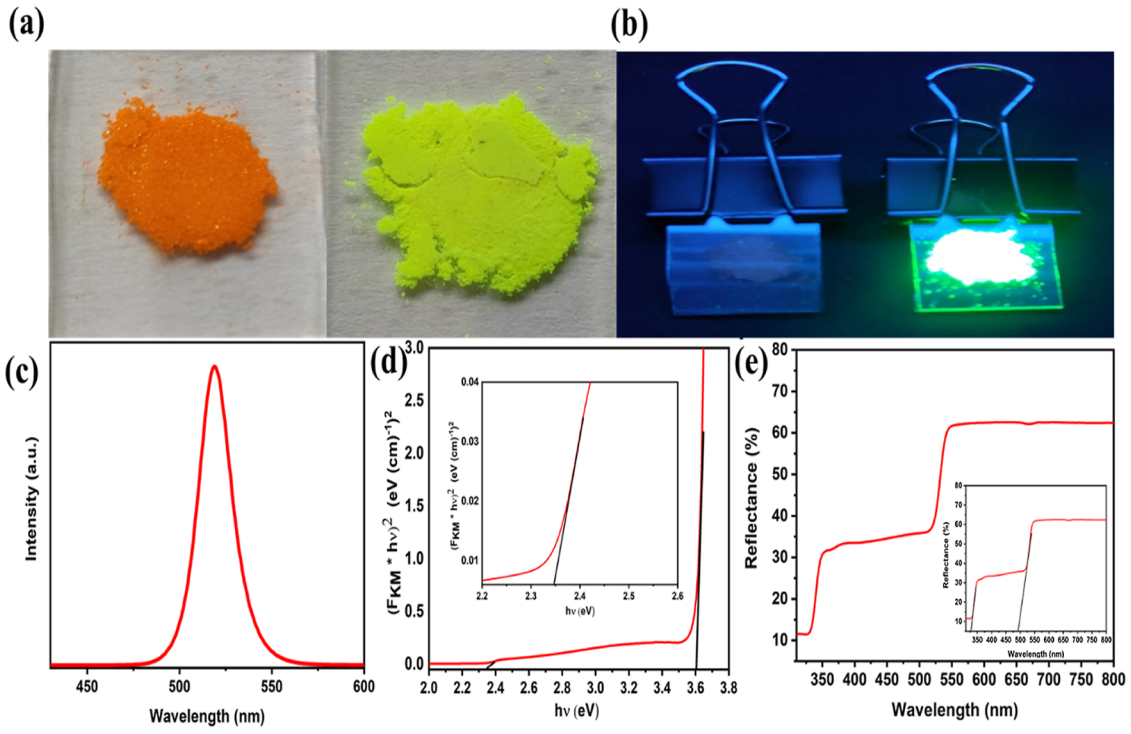


**Figure 3.** Optical images of $CsPbBr_3$ and $Cs_4PbBr_6$ microcrystals, respectively, under (a) ambient light, (b) UV irradiation, (c) solid-state PL emission spectra, (d) Kubelka Munk plot manifesting direct band gaps of 2.34, and 3.6 eV corresponding to the mid band gap state and from intrinsic band gap of the material, respectively. The inset figure shows the enlarged view of the KM plot of the mid band gap state. (e) Reflectance plot of $Cs_4PbBr_6$ microcrystals. Inset figure shows the same plot extrapolated to *x* axis to indicate the wavelength corresponding to absorption band.

According to the literature, there are two major possibilities associated with green emission. The first one discusses the possibility of impurity phases of $CsPbBr_3$ nanocrystals in trace amounts embedded in the matrix of $Cs_4PbBr_6$ as the reason for emission.[56,57] But from XRD data, it is evident that the powder form is a pure phase of $Cs_4PbBr_6$ without any impurity phases. On the other hand, some literature acknowledges the green emission as the inherent property of 0D $Cs_4PbBr_6$ arising due to the intrinsically available defect states that are inherent within the band gap, in turn acting as radiative recombination centers causing robust emission.[12,58] But, from the observed PL emission peak at 519 nm, the corresponding energy state was calculated to be 2.39 eV according to eq 1, Section 2.5. Literature discusses the possibility of formation of sub or mid band gap state around 2.4 eV due to the existence of localized Br vacancies in the 0D crystals.[59,60] Though the intrinsic band gap of $Cs_4PbBr_6$ is in the range of 3.2−3.9 eV, this defect energy level of Br vacancy provides a sub band gap state enabling photons of lower energy to excite electrons which can possibly act as major recombination centers[59] and thereby causing green emission, which synchronize well with the calculated value of 2.39 eV. Moreover, the possibility of this is supported by DFT calculations which explain the presence of localized bromine vacancies in the 0D crystals capturing the exciton and acting as recombination centers. Till date, the exact mechanism behind the origin of green luminescence is still a matter of controversy among the researchers.[14,61] The comparison of PL spectra of both the microcrystals is given in Figure S5a. The comparison PL substantiates that the 3D counterpart exhibits low PL due to lower exciton binding energy (19−60 meV) causing the free charge carriers to dissociate and travel all through the octahedra which are corner shared thereby reducing the probability of fast radiative recombination.[3,62,63] The PL spectra at different excitation wavelengths (Figure S5b) imply that the maximum emission intensity occurs at 365 nm compared to all other wavelengths showing its wavelength dependence. It is clear that $Cs_4PbBr_6$ is a direct band gap material with its intrinsic band gap ranging from 3.2 to 3.9 eV.[6] But due to the existence of Br vacancy, $Cs_4PbBr_6$ portrays two band gaps of (i) ∼2.34 eV associated with the defect state sub band gap and (ii) 3.6 eV attributed to its intrinsic band gap (Figure 3d) calculated as per $Cs_4PbBr_6$ by Kubelka Munk theory.[17,43,64] The inset of Figure 3d shows the sub band gap plot arising due to Br vacancies corresponding to the band gap of 2.34 eV. The calculated values for the band gap were slightly less when compared to the theoretical value of 3.95 eV $Cs_4PbBr_6$.[4,65,66] The DRS for the 0D microcrystals are given in Figure 3e. The reflectance plot contains two peaks with respect to two absorption regions corresponding to the two band gaps. The inset shows the same reflectance plot when extrapolated to *x*-axis to indicate the wavelength corresponding to the absorption band. The line intersects the *x*-axis at wavelengths—329 and 493 nm. Using eq 1 of Section 2.5, the band gap was calculated to be ∼3.76, and ∼2.51 eV, corresponding to intrinsic and defect state band gaps, respectively, as discussed in the manuscript which is in agreement with previously mentioned literature. After crossing the absorption edge occurring beyond ∼530 nm,[67] 60% of the light is reflected by the sample. The Kubelka Munk plot and reflectance spectra of $CsPbBr_3$ microcrystals are given in Figure S5d,e respectively. The band gap of $CsPbBr_3$ was calculated to be 2.26 eV which is in agreement with the theoretical value ranging from 0.79 to 2.54 eV. From the reflectance plot (Figure S5e), it is evident that the sample reflects ∼80% of light after the absorption edge of 553 nm.[68] From the optical and emission property analysis of both the microcrystals, it is


https://doi.org/10.1021/acsomega.2c05862
ACS Omega 2023, 8, 4616−4626

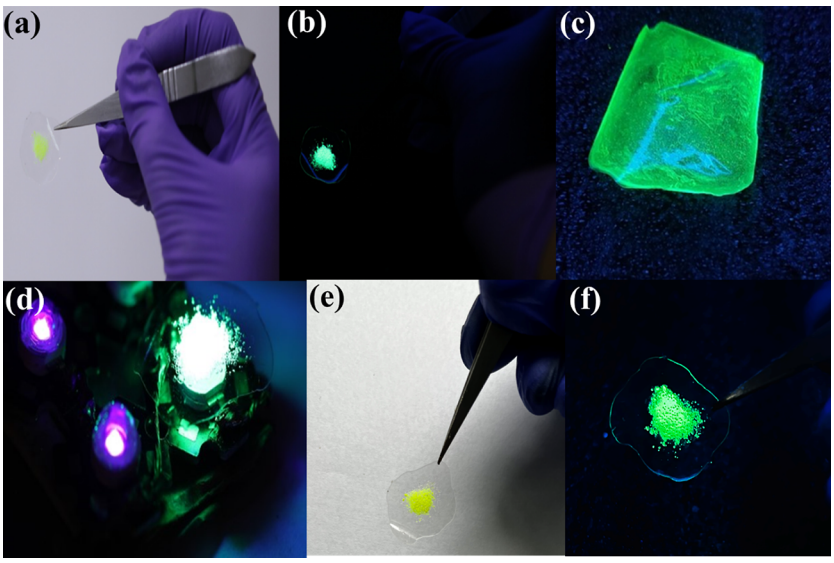


**Figure 4.** (a and b) Photographs of the $Cs_4PbBr_6$@PMMA film under daylight and 365 nm UV irradiation (right figure) on day 1, (c) $Cs_4PbBr_6$@PMMA film directly made from precursor solution when irradiated under UV light. (d) Camera photograph of $Cs_4PbBr_6$@PMMA film on top of violet LED. (e and f) Photographs of the $Cs_4PbBr_6$@PMMA film under the daylight and 365 nm UV irradiation respectively, on day 400.

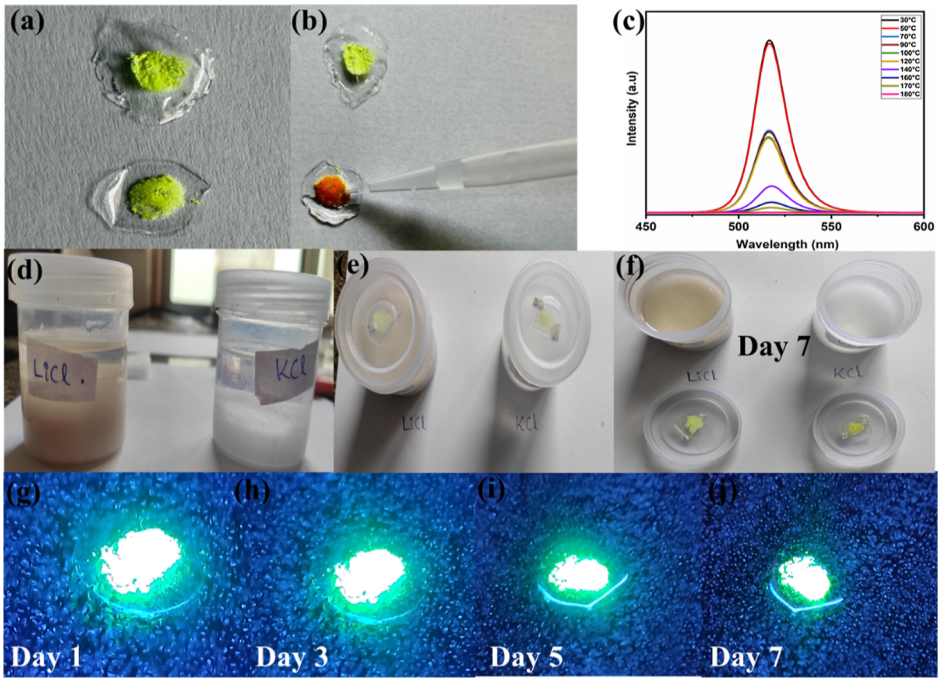


**Figure 5.** Images of (a and b) $Cs_4PbBr_6$@PMMA film when tested for stability against water. (c) PL emission spectra of the $Cs_4PbBr_6$@PMMA film at various temperatures ranging from 30 to 180 °C. (d–f) Saturated solution of LiCl and KCl and the photograph of the $Cs_4PbBr_6$@PMMA film when exposed to two extreme humidity conditions indicating no phase transformation even after 7 days. (g–j) $Cs_4PbBr_6$@PMMA film by continuously exposing it under 365 nm UV irradiation for 7 days.

well evident that $Cs_4PbBr_6$ can serve as a powerful claimant in several optoelectronic applications including LEDs, backlight, and liquid crystal displays remarkably owing to its excellent emissive nature when compared to its 3D counterpart.

**3.4. Application of $Cs_4PbBr_6$@PMMA Film as Color Converters.** The photographs of the flexible free-standing $Cs_4PbBr_6$@PMMA film under daylight and UV light illumination are given in Figure 4a,b. Herein, we have developed a free-standing perovskite-polymer film that would emit green light producing a green emission when placed over a violet LED. The $Cs_4PbBr_6$@PMMA film was also made from the precursor solution giving stable green emission (Figure 4c). The deposited film was found to be mechanically flexible and resistant to moisture threats. Figure 4d shows the $Cs_4PbBr_6$@PMMA film over violet LED engendering green light. The comparison of PL spectra on day 1 versus day 180 of the $Cs_4PbBr_6$ microcrystals (Figure S5c) portrays the stability of the fluorophore powder over 6 months engendering a stable emission intensity. To check the stability of the $Cs_4PbBr_6$@PMMA film, the film was kept out in normal room temperature conditions for more than a year (400 days) and was found that it retained stability without any phase transition (Figure 4e,f).



https://doi.org/10.1021/acsomega.2c05862
ACS Omega 2023, 8, 4616−4626

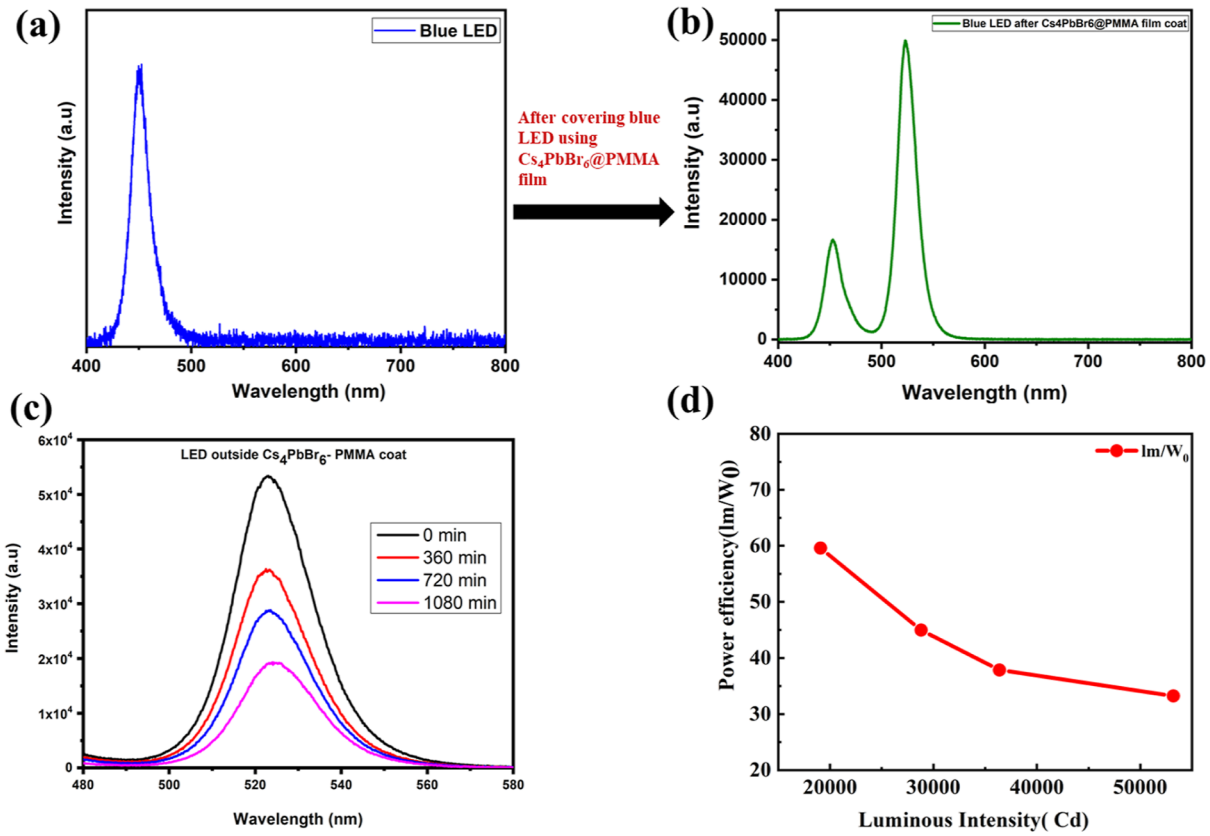


**Figure 6.** (a and b) Image on the left depicts the intensity of bare blue LED and image on the right depicts the intensity of blue LED after coating with the $Cs_4PbBr_6$@PMMA film portraying the green emission at ~524 nm. (c) Wavelength vs intensity plot of the $Cs_4PbBr_6$@PMMA film over commercial blue LED as a function of time. (d) Ratio of $l_m/W_0$ from power efficiency curve.

The major concern regarding any perovskite material is its stability against moisture and water. Herein, the PMMA matrix provides better protection to the perovskite microcrystal, thereby preventing the attack of moisture and water. PMMA is highly utilized as a synthetic polymer due to its flexibility and ability to form a transparent film when dissolved. PMMA is also resistant to UV radiation which is the major advantage for opting PMMA as an embedding substrate.[69,70] Moreover, PMMA is highly hydrophobic in nature so it does not allow water molecules to decompose the perovskite structure which maintains the stability of $Cs_4PbBr_6$ powder when used as a coating layer over the top of fluorophore powder. It is clear that embedding microcrystals in the PMMA polymer matrix could efficiently protect the perovskite from moisture attacks and enhance its stability without undergoing any phase transformations.

**3.5. Stability Study of $Cs_4PbBr_6$ Powder against Water, Temperature, Humidity, and UV Radiation.** The stability of the as-synthesized microcrystals was analyzed against water, temperature, humidity, and UV radiation. For checking the stability of the fluorophore against water, the $Cs_4PbBr_6$@PMMA film was taken and 5 $\mu$L water was added on the top of the film using a micropipette (Figure 5a,b). It is evident that soon after adding water dropwise, the green color of the powder turned to orange indicating the direct transformation from 0D to 3D phase which is non-luminescent. Hence, it agrees with the nature of perovskite and its instability when exposed to an aqueous environment. In order to study the stability and PL intensity dependence concerning the increase in temperature, the $Cs_4PbBr_6$@PMMA film was heated on a hot plate at temperatures ranging from 30 to 180 °C in open air, and PL spectra were taken by using an excitation wavelength of 365 nm. From the PL spectra of Figure 5c, it is evident that the fluorophore powder showed a reduction in PL attributed to the enhanced non-radiative recombination rates which dominate the rate of radiative recombination at elevated temperatures.[14,71] After 120 °C, there was an abrupt decrease in PL intensity and at 180 °C, the emission intensity was close to zero. To check the reversibility, the powder was cooled back to room temperature and PL was taken as shown in Figure S6. The PL spectra after cooling down to room temperature retained 51% of their original intensity suggesting appreciable thermal stability. The $Cs_4PbBr_6$@PMMA was exposed to different humidity conditions for seven days to analyze the stability against moisture. For this, saturated solutions of LiCl and KCl were prepared corresponding to 11 and 84% RH conditions, respectively. Figure 5d–f substantiates that no transformation or phase change happened to the fluorophore powder even after being exposed to two extreme humidity conditions indicating its ability to withstand moisture. Finally, the UV stability was tested by placing the $Cs_4PbBr_6$@PMMA under the UV chamber for 7 days exposed to UV radiation of wavelength 365 nm. There is no damage caused to the film and the fluorescence is still maintained even after 7 days confirming the excellent stability after continuous exposure to UV radiation (Figure 5g–j).

**3.6. Intensity Analysis of $Cs_4PbBr_6$@PMMA Film over Commercial Blue LED.** The intensity analysis was carried out using an optical fiber employing a blue LED and the PMMA


https://doi.org/10.1021/acsomega.2c05862
ACS Omega 2023, 8, 4616−4626

coated fluorophore powder of $Cs_4PbBr_6$. Figure 6a,b shows the intensity versus wavelength analysis of bare blue LED and the change in intensity of blue LED after employing the $Cs_4PbBr_6$@PMMA coat as the top cover over the blue LED. It is evident that after covering with $Cs_4PbBr_6$@PMMA, the intensity of blue LED faces a reduction along with an increase of intensity in the green region. The analysis shows that the usage of the fluorophore powder can produce an emission of wavelength ∼525 nm which is in the green region. Figure 6c depicts the intensity versus wavelength plot of the $Cs_4PbBr_6$@PMMA coat over commercial blue LED as a function of time. As time progresses, even after 18 h, there is only ∼50% reduction in the intensity of emitted light despite continuous operation. This indicates the practical application of the fluorophore powder for long hours of operation for backlight applications. From the power efficiency curve, we can see that a maximum of 59.6 $L_m/W_o$ can be achieved at 19,000 Cd luminous intensity for the $Cs_4PbBr_6$@PMMA film (Figure 6d). The calculations for power efficiency versus luminous intensity is given in Table S2. Hence, it is evident from this analysis that the $Cs_4PbBr_6$ fluorophore powder possesses the ability to convert light from blue to green region along with polymer protection and reveal its potential application as a color converter. Also, this PMMA coated fluorophore powder put forth a compact base in utilizing them as backlights to produce a desired intense green emission. The use of PMMA matrix helped in overcoming the inhomogeneity of microcrystals to a larger extent. By uniformly spreading the $Cs_4PbBr_6$ microcrystals over PMMA which has a smooth surface, a homogenous film can be made that would substantiate the inhomogeneity of microcrystals thereby its application in backlight displays producing emission. These microcrystals can also be combined together with red and blue fluorophores[72] to produce white light emissions and even as color converters.

## 4. CONCLUSIONS

This work is all about the large-scale synthesis of fluorophore microcrystal powder from gram to kilogram scale, using a very simple and single-step method. The major advantage of this synthesis route is that there are no limitations since the experimental yield was found to be 99.4% signifying that the entire precursor got converted to the $Cs_4PbBr_6$ microcrystal without leaving them unreacted. The as-synthesized powder can work as an excellent color-converters that can be employed in UV emitting LEDs. From this analysis, it is well evident that the microcrystals possess the property of green emission whenever it is irradiated with a UV source. The fabricated $Cs_4PbBr_6$@PMMA fluorophore film possesses appreciable stability of 400 days attributed to the role of PMMA in enhancing stability and enables its usage for a longer period without causing any phase transformations. Therefore, the 0D $Cs_4PbBr_6$ microcrystal fluorophore powder can serve as a backlight to produce a desired robust green emission. In addition to that, these micro-sized green fluorophore powder and film in combination with red fluorophores can be used as a coating over blue LEDs to produce white light emission in white light emitting diodes which extends the forward looking perspective of the work.

## ASSOCIATED CONTENT

### Supporting Information

The Supporting Information is available free of charge at https://pubs.acs.org/doi/10.1021/acsomega.2c05862.

Synthesis of PMMA—toluene solution followed by the scheme and details of fabrication of free-standing $Cs_4PbBr_6$@PMMA film; XRD analysis of $Cs_4PbBr_6$@PMMA, additional characterization results of $CsPbBr_3$ microcrystals—XRD, SEM, and its optical properties; EDX, elemental mapping, chemical composition, and emission behavior of $Cs_4PbBr_6$ microcrystals with comparison PL studies (PDF)

## AUTHOR INFORMATION


### Corresponding Author

**Sudip K. Batabyal** − *Department of Sciences, Amrita School of Physical Sciences, Coimbatore, Amrita Vishwa Vidyapeetham, Coimbatore 641112 Tamil Nadu, India; Amrita Center for Industrial Research & Innovation (ACIRI), Amrita School of Engineering, Coimbatore, Amrita Vishwa Vidyapeetham, Coimbatore 641112 Tamil Nadu, India;* orcid.org/0000-0003-0615-9576; Email: s_batabyal@cb.amrita.edu

### Authors

**Swapnika Suresh** − *Department of Sciences, Amrita School of Physical Sciences, Coimbatore, Amrita Vishwa Vidyapeetham, Coimbatore 641112 Tamil Nadu, India*

**Mohan Raj Subramaniam** − *Department of Sciences, Amrita School of Physical Sciences, Coimbatore, Amrita Vishwa Vidyapeetham, Coimbatore 641112 Tamil Nadu, India*

**Sobhan Hazra** − *School of Material Science and Technology, Indian Institute of Technology (BHU), Varanasi 221005 Uttar Pradesh, India*

**Bhola Nath Pal** − *School of Material Science and Technology, Indian Institute of Technology (BHU), Varanasi 221005 Uttar Pradesh, India*

Complete contact information is available at: https://pubs.acs.org/10.1021/acsomega.2c05862


### Notes

The authors declare the following competing financial interest(s): The authors want to declare that one patent was applied from Amrita Vishwa Vidyapeetham based on that work.

## ACKNOWLEDGMENTS

The authors thank the Department of Science and Technology, Government of India, for constantly supporting this research program. The authors also acknowledge the support of INSPIRE Fellowship, Department of Science and Technology, Government of India.

## REFERENCES

(1) Chen, M.; Yang, S.; Yuan, Y.; Shen, X.; Liu, Y.; Wang, Q.; Cao, D.; Xu, C. Thermal Quenching and Antiquenching of Photoluminescence in Solution-Grown Cs4PbBr6 Perovskite Single Crystals. *J. Phys. Chem. C* **2021**, *125*, 11278−11284.

(2) Song, Y. H.; Choi, S. H.; Park, W. K.; Yoo, J. S.; Kwon, S. B.; Kang, B. K.; Park, S. R.; Seo, Y. S.; Yang, W. S.; Yoon, D. H. Innovatively Continuous Mass Production Couette-taylor Flow: Pure Inorganic Green-Emitting Cs4PbBr6 Perovskite Microcrystal for display technology. *Sci. Rep.* **2018**, *8*, 2−7.

(3) Saidaminov, M. I.; Almutlaq, J.; Sarmah, S.; Dursun, I.; Zhumekenov, A. A.; Begum, R.; Pan, J.; Cho, N.; Mohammed, O. F.; Bakr, O. M. Pure Cs4PbBr6: Highly Luminescent Zero-Dimensional Perovskite Solids. *ACS Energy Lett.* **2016**, *1*, 840−845.

(4) La Porta, F. A.; Masi, S. Solvent-Mediated Structural Evolution Mechanism from Cs 4 PbBr 6 to CsPbBr 3 Crystals. *Nanomanufacturing* **2021**, *1*, 67−74.
(5) Ray, A.; Maggioni, D.; Baranov, D.; Dang, Z.; Prato, M.; Akkerman, Q. A.; Goldoni, L.; Caneva, E.; Manna, L.; Abdelhady, A. L. Green-Emitting Powders of Zero-Dimensional Cs4PbBr6: Delineating the Intricacies of the Synthesis and the Origin of Photoluminescence. *Chem. Mater.* **2019**, *31*, 7761−7769.
(6) Shi, Z.; Yang, Y.; Sun, X. Y.; Lang, F.; Lin, L. Improvement in optical properties of Cs4PbBr6 nanocrystals using aprotic polar purification solvent. *RSC Adv.* **2021**, *11*, 16453−16460.
(7) Subramaniam, M. R.; Pramod, A. K.; Hevia, S. A.; Batabyal, S. K. Enhanced Photoluminescence Quantum Yield, Lifetime, and Photodetector Responsivity of CsPbBr3 Quantum Dots via Antimony Tribromide Post-Treatment. *J. Phys. Chem. C* **2022**, *126*, 1462−1470.
(8) Pramod, A. K.; Raj Subramaniam, M. R.; Hevia, S. A.; Batabyal, S. K. Synthesis of Lead-Free Cs3Sb2Cl3Br6 Halide Perovskite through Solution Processing Method for Self-Powered Photodetector Applications. *Mater. Lett.* **2022**, *306*, 130874.
(9) Chen, Y. M.; Zhou, Y.; Zhao, Q.; Zhang, J. Y.; Ma, J. P.; Xuan, T. T.; Guo, S. Q.; Yong, Z. J.; Wang, J.; Kuroiwa, Y.; Moriyoshi, C.; Sun, H. T. Cs4PbBr6/CsPbBr3 Perovskite Composites with Near-Unity Luminescence Quantum Yield: Large-Scale Synthesis, Luminescence and Formation Mechanism, and White Light-Emitting Diode Application. *ACS Appl. Mater. Interfaces* **2018**, *10*, 15905−15912.
(10) Sun, J. Y.; Rabouw, F. T.; Yang, X. F.; Huang, X. Y.; Jing, X. P.; Ye, S.; Zhang, Q. Y. Facile Two-Step Synthesis of All-Inorganic Perovskite CsPbX3 (X = Cl, Br, and I) Zeolite-Y Composite Phosphors for Potential Backlight Display Application. *Adv. Funct. Mater.* **2017**, *27*, 1704371.
(11) Seth, S.; Samanta, A. Fluorescent Phase-Pure Zero-Dimensional Perovskite-Related Cs4PbBr6 Microdisks: Synthesis and Single-Particle Imaging Study. *J. Phys. Chem. Lett.* **2017**, *8*, 4461−4467.
(12) De Bastiani, M.; Dursun, I.; Zhang, Y.; Alshankiti, B. A.; Miao, X. H.; Yin, J.; Yengel, E.; Alarousu, E.; Turedi, B.; Almutlaq, J. M.; Saidaminov, M. I.; Mitra, S.; Gereige, I.; AlSaggaf, A.; Zhu, Y.; Han, Y.; Roqan, I. S.; Bredas, J. L.; Mohammed, O. F.; Bakr, O. M. Inside Perovskites: Quantum Luminescence from Bulk Cs4PbBr6 Single Crystals. *Chem. Mater.* **2017**, *29*, 7108−7113.
(13) Xu, L.; Li, J.; Fang, T.; Zhao, Y.; Yuan, S.; Dong, Y.; Song, J. Synthesis of stable and phase-adjustable CsPbBr3@Cs4PbBr6 nanocrystals via novel anion-cation reactions. *Nanoscale Adv.* **2019**, *1*, 980−988.
(14) Chen, D.; Wan, Z.; Chen, X.; Yuan, Y.; Zhong, J. Large-scale room-temperature synthesis and optical properties of perovskite-related Cs4PbBr6fluorophores. *J. Mater. Chem. C* **2016**, *4*, 10646−10653.
(15) Zhang, J.; Wang, A.; Kong, L.; Zhang, L.; Deng, Z. Controlled Synthesis of Zero-Dimensional Phase-Pure Cs4PbBr6 Perovskites Crystals with High Photoluminescence Quantum Yield. *J. Alloys Compd.* **2019**, *797*, 1151−1156.
(16) He, Q.; Mei, E.; Liang, X.; Xiang, W. Ultrastable PVB Films-Protected CsPbBr3/Cs4PbBr6 Perovskites with High Color Purity for Nearing Rec. 2020 Standard. *Chem. Eng. J.* **2021**, *419*, 129529.
(17) Wei, Y.; Sun, R.; Li, Y.; Zhang, Y.; Lu, Y.; Li, X.; Chen, G.; Cao, B.; Li, C.; Zeng, H. Single-Solvent, Ligand-Free, Gram-Scale Synthesis of Cs4PbBr6 Perovskite Solids with Robust Green Photoluminescence. *ChemNanoMat* **2020**, *6*, 258−266.
(18) Fu, L.; Zi, Y.; Bai, X.; Xiao, D.; Haider, A. A.; Qiu, J.; Song, Z.; Cun, Y.; Yang, Z. Preparation and Photoluminescence of Cs4PbBr6 Perovskite Quantum Dot Embedded in Borophosphate Glass. *J. Alloys Compd.* **2022**, *911*, 165004.
(19) Feng, S.; Qin, Q.; Han, X.; Zhang, C.; Wang, X.; Yu, T.; Xiao, M. Universal Existence of Localized Single-Photon Emitters in the Perovskite Film of All-Inorganic CsPbBr 3 Microcrystals. *Adv. Mater.* **2022**, *34*, 2106278.
(20) Dirin, D. N.; Cherniukh, I.; Yakunin, S.; Shynkarenko, Y.; Kovalenko, M. V. Solution-Grown CsPbBr3 Perovskite Single Crystals for Photon Detection. *Chem. Mater.* **2016**, *28*, 8470−8474.
(21) Thumu, U.; Piotrowski, M.; Owens-Baird, B.; Kolen'ko, Y. V. Zero-Dimensional Cesium Lead Halide Perovskites: Phase Transformations, Hybrid Structures, and Applications. *J. Solid State Chem.* **2019**, *271*, 361−377.
(22) Li, X.; Wen, Z.; Ding, S.; Fang, F.; Xu, B.; Sun, J.; Liu, C.; Wang, K.; Sun, X. W. Facile In Situ Fabrication of Cs4PbBr6/CsPbBr3 Nanocomposite Containing Polymer Films for Ultrawide Color Gamut Displays. *Adv. Opt. Mater.* **2020**, *8*, 2000232.
(23) Naresh, V.; Kim, B. H.; Lee, N. Synthesis of CsPbX3 (X = Cl/Br, Br, and Br/I)@SiO2/PMMA Composite Films as Color-Conversion Materials for Achieving Tunable Multi-Color and White Light Emission. *Nano Res.* **2021**, *14*, 1187−1194.
(24) Corzo, D.; Tostado-Blázquez, G.; Baran, D. Flexible Electronics: Status, Challenges and Opportunities. *Front. Electron.* **2020**, *1*, 1−13.
(25) Zhou, Y.; Qiu, X.; Wan, Z.; Long, Z.; Poddar, S.; Zhang, Q.; Ding, Y.; Chan, C. L. J.; Zhang, D.; Zhou, K.; Lin, Y.; Fan, Z. Halide-Exchanged Perovskite Photodetectors for Wearable Visible-Blind Ultraviolet Monitoring. *Nano Energy* **2022**, *100*, 107516.
(26) Dong, R.; Fang, Y.; Chae, J.; Dai, J.; Xiao, Z.; Dong, Q.; Yuan, Y.; Centrone, A.; Zeng, X. C.; Huang, J. High-Gain and Low-Driving-Voltage Photodetectors Based on Organolead Triiodide Perovskites. *Adv. Mater.* **2015**, *27*, 1912−1918.
(27) Xu, W.; Lei, G.; Tao, C.; Zhang, J.; Liu, X.; Xu, X.; Lai, W. Y.; Gao, F.; Huang, W. Precisely Controlling the Grain Sizes with an Ammonium Hypophosphite Additive for High-Performance Perovskite Solar Cells. *Adv. Funct. Mater.* **2018**, *28*, 1802320.
(28) Zhang, Q.; Shang, Q.; Su, R.; Do, T. T. H.; Xiong, Q. Halide Perovskite Semiconductor Lasers: Materials, Cavity Design, and Low Threshold. *Nano Lett.* **2021**, *21*, 1903−1914.
(29) Zhang, F.; Min, H.; Zhang, Y.; Kuang, Z.; Wang, J.; Feng, Z.; Wen, K.; Xu, L.; Yang, C.; Shi, H.; Zhuo, C.; Wang, N.; Chang, J.; Huang, W.; Wang, J. Vapor-Assisted In Situ Recrystallization for Efficient Tin-Based Perovskite Light-Emitting Diodes. *Adv. Mater.* **2022**, *34*, 2203180.
(30) Ren, K.; Yue, S.; Li, C.; Fang, Z.; Gasem, K. A. M.; Leszczynski, J.; Qu, S.; Wang, Z.; Fan, M. Metal Halide Perovskites for Photocatalysis Applications. *J. Mater. Chem. A* **2022**, *10*, 407−429.
(31) Zhang, C.; Kuang, D. B.; Wu, W. Q. A Review of Diverse Halide Perovskite Morphologies for Efficient Optoelectronic Applications. *Small Methods* **2020**, *4*, 1900662.
(32) Stranks, S. D.; Eperon, G. E.; Grancini, G.; Menelaou, C.; Alcocer, M. J. P.; Leijtens, T.; Herz, L. M.; Petrozza, A.; Snaith, H. J. Electron-Hole Diffusion Lengths Exceeding 1 Micrometer in an Organometal Trihalide Perovskite Absorber. *Science* **2013**, *342*, 341−344.
(33) Fakharuddin, A.; Gangishetty, M. K.; Abdi-Jalebi, M.; Chin, S. H.; bin Mohd Yusoff, A. R.; Congreve, D. N.; Tress, W.; Deschler, F.; Vasilopoulou, M.; Bolink, H. J. Perovskite Light-Emitting Diodes. *Nat. Electron.* **2022**, *5*, 203−216.
(34) Sun, Y.; Zhang, L.; Wang, N.; Zhang, S.; Cao, Y.; Miao, Y.; Xu, M.; Zhang, H.; Li, H.; Yi, C.; Wang, J.; Huang, W. The Formation of Perovskite Multiple Quantum Well Structures for High Performance Light-Emitting Diodes. *npj Flexible Electron.* **2018**, *2*, 12.
(35) Yoon, Y. J.; Kim, J. Y. A Recent Advances of Blue Perovskite Light Emitting Diodes for next Generation Displays. *J. Semicond.* **2021**, *42*, 101608.
(36) Quan, L. N.; Yuan, M.; Comin, R.; Voznyy, O.; Beauregard, E. M.; Hoogland, S.; Buin, A.; Kirmani, A. R.; Zhao, K.; Amassian, A.; Kim, D. H.; Sargent, E. H. Ligand-Stabilized Reduced-Dimensionality Perovskites. *J. Am. Chem. Soc.* **2016**, *138*, 2649−2655.
(37) Bai, X.; Meng, L.; Zhou, N.; Zheng, J.; Yu, X. F.; Chu, P. K.; Xiao, J. J.; Zou, B.; Li, J. In Situ Preparation of Mn-Doped Perovskite Nanocrystalline Films and Application to White Light Emitting Devices. *J. Colloid Interface Sci.* **2022**, *606*, 1163−1169.
(38) Zhang, Y.; Zhang, B.; Fu, Y.; Han, Y.; Zhang, T.; Zhang, L.; Guo, J.; Zhang, X. An Ultrastable Perovskite-Polymer Exciplex through Self Energy-Level Adaption for under-Water Light-Emitting Devices. *J. Mater. Chem. C* **2022**, *10*, 8609−8616.


https://doi.org/10.1021/acsomega.2c05862
*ACS Omega* 2023, 8, 4616−4626

(39) Huang, J. C.; Chu, Y. P.; Wei, M.; Deanin, R. D. Comparison of Epoxy Resins for Applications in Light-Emitting Diodes. *Adv. Polym. Technol.* **2004**, *23*, 298−306.
(40) Venkatachalaiah, K. N.; Nagabhushana, H.; Darshan, G. P.; Basavaraj, R. B.; Daruka Prasad, B. D.; Sharma, S. C. Blue light emitting Y 2 O 3 :Tm 3+ nanophosphors with tunable morphology obtained by bio-surfactant assisted sonochemical route. *Spectrochim. Acta, Part A* **2017**, *184*, 89−100.
(41) Venkatachalaiah, K. N.; Nagabhushana, H.; Darshan, G. P.; Basavaraj, R. B.; Prasad, B. D.; Sharma, S. C. Structural, morphological and photometric properties of sonochemically synthesized Eu 3+ doped Y 2 O 3 nanophosphor for optoelectronic devices. *Mater. Res. Bull.* **2017**, *94*, 442−455.
(42) Venkatachalaiah, K. N.; Nagabhushana, H.; Darshan, G. P.; Basavaraj, R. B.; Prasad, B. D. Novel and highly efficient red luminescent sensor based SiO2@Y2O3:Eu3+, M+ (M+= Li, Na, K) composite core-shell fluorescent markers for latent fingerprint recognition, security ink and solid state lightning applications. *Sens. Actuators, B* **2017**, *251*, 310−325.
(43) Venkataravanappa, M.; Venkatachalaiah, K. N.; Basavaraj, R. B.; Prasanna Kumar, J. B.; Daruka Prasad, B.; Nagabhushana, H. Photoluminescence Properties of Dy3+ Activated Ca2SiO4 Nano-phosphor for WLED Applications. *Inorg. Nano-Met. Chem.* **2018**, *48*, 107−109.
(44) Baxamusa, S. H.; Stadermann, M.; Aracne-Ruddle, C.; Nelson, A. J.; Chea, M.; Li, S.; Youngblood, K.; Suratwala, T. I. Enhanced Delamination of Ultrathin Free-Standing Polymer Films via Self-Limiting Surface Modification. *Langmuir* **2014**, *30*, 5126−5132.
(45) Yang, G.; Fan, Q.; Chen, B.; Zhou, Q.; Zhong, H. Reprecipitation Synthesis of Luminescent CH3NH3PbBr3/NaNO3 Nanocomposites with Enhanced Stability. *J. Mater. Chem. C* **2016**, *4*, 11387−11391.
(46) Xiang, H.; Wang, R.; Chen, J.; Li, F.; Zeng, H. Research Progress of Full Electroluminescent White Light-Emitting Diodes Based on a Single Emissive Layer. *Light: Sci. Appl.* **2021**, *10*, 206.
(47) Xuan, T.; Guo, S.; Bai, W.; Zhou, T.; Wang, L.; Xie, R. J. Ultrastable and Highly Efficient Green-Emitting Perovskite Quantum Dot Composites for Mini-LED Displays or Backlights. *Nano Energy* **2022**, *95*, 107003.
(48) Lin, Y. C.; Karlsson, M.; Bettinelli, M. Inorganic Phosphor Materials for Lighting. *Top. Curr. Chem.* **2016**, *374*, 374−421.
(49) Jafar, M. M. A. G.; Saleh, M. H.; Ahmad, M. J. A.; Bulos, B. N.; Al-Daraghmeh, T. M. Retrieval of Optical Constants of Undoped Amorphous Selenium Films from an Analysis of Their Normal-Incidence Transmittance Spectra Using Numeric PUMA Method. *J. Mater. Sci.: Mater. Electron.* **2016**, *27*, 3281−3291.
(50) Abdullahi, S. S.; Güner, S.; Koseoglu, Y.; Musa, I. M.; Adamu, B. I.; Abdulhamid, M. I. Simple Method For The Determınatıon of Band Gap of a Nanopowdered Sample Usıng Kubelka Munk Theory. *J. Niger. Assoc. Math. Phys.* **2016**, *35*, 241−246.
(51) Rykowski, R.; Kostal, H. Novel Approach for LED Luminous Intensity Measurement. *Light. Diodes Res. Manuf. Appl. XII.* **2008**, *6910*, 69100C.
(52) Nguyen, L. A. T.; Minh, D. N.; Zhang, D.; Wang, L.; Kim, J.; Kang, Y. Pressure-Induced Selective Amorphization of CsPbBr3 for the Purification of Cs4PbBr6. *J. Phys. Chem. C* **2020**, *124*, 22291−22297.
(53) Riesen, N.; Lockrey, M.; Badek, K.; Riesen, H. On the Origins of the Green Luminescence in the "Zero-Dimensional Perovskite" Cs4PbBr6: Conclusive Results from Cathodoluminescence Imaging. *Nanoscale* **2019**, *11*, 3925−3932.
(54) Møller, C. K. The Structure of Perovskite-like Cesium Plumbo Trihalides. *Mat.-Fys. Medd. - K. Dan. Vidensk. Selsk.* **1959**, *32*, 1−27.
(55) Xu, W. L.; Bradley, S. J.; Xu, Y.; Zheng, F.; Hall, C. R.; Ghiggino, K. P.; Smith, T. A. Highly Efficient Radiative Recombination in Intrinsically Zero-Dimensional Perovskite Micro-Crystals Prepared by Thermally-Assisted Solution-Phase Synthesis. *RSC Adv.* **2020**, *10*, 43579−43584.
(56) Liu, Z.; Bekenstein, Y.; Ye, X.; Nguyen, S. C.; Swabeck, J.; Zhang, D.; Lee, S. T.; Yang, P.; Ma, W.; Alivisatos, A. P. Ligand Mediated Transformation of Cesium Lead Bromide Perovskite Nanocrystals to Lead Depleted Cs4PbBr6 Nanocrystals. *J. Am. Chem. Soc.* **2017**, *139*, 5309−5312.
(57) Han, D.; Shi, H.; Ming, W.; Zhou, C.; Ma, B.; Saparov, B.; Ma, Y. Z.; Chen, S.; Du, M. H. Unraveling Luminescence Mechanisms in Zero-Dimensional Halide Perovskites. *J. Mater. Chem. C* **2018**, *6*, 6398−6405.
(58) Yin, J.; Zhang, Y.; Bruno, A.; Soci, C.; Bakr, O. M.; Brédas, J. L.; Mohammed, O. F. Intrinsic Lead Ion Emissions in Zero-Dimensional Cs4PbBr6 Nanocrystals. *ACS Energy Lett.* **2017**, *2*, 2805−2811.
(59) Luo, B.; Li, H.; Wang, Y.; Wang, L.; Li, J.; Huang, J.; Ye, Z. Liquid Diffused Separation Induced Crystallization to efficiently grow centimeter-sized diamond-like Cs4PbBr6 crystals for light-emitting applications. *J. Lumin.* **2022**, *251*, 119195.
(60) Shin, M.; Nam, S. W.; Sadhanala, A.; Shivanna, R.; Anaya, M.; Jiménez-Solano, A.; Yoon, H.; Jeon, S.; Stranks, S. D.; Hoye, R. L. Z.; Shin, B. Understanding the Origin of Ultrasharp Sub-Band gap Luminescence from Zero-Dimensional Inorganic Perovskite Cs4PbBr6. *ACS Appl. Energy Mater.* **2020**, *3*, 192−199.
(61) Qin, Z.; Dai, S.; Hadjiev, V. G.; Wang, C.; Xie, L.; Ni, Y.; Wu, C.; Yang, G.; Chen, S.; Deng, L.; Yu, Q.; Feng, G.; Wang, Z. M.; Bao, J. Revealing the Origin of Luminescence Center in 0D Cs4PbBr6 Perovskite. *Chem. Mater.* **2019**, *31*, 9098−9104.
(62) Manser, J. S.; Kamat, P. V. Band Filling with Free Charge Carriers in Organometal Halide Perovskites. *Nat. Photonics* **2014**, *8*, 737−743.
(63) Miyata, A.; Mitioglu, A.; Plochocka, P.; Portugall, O.; Wang, J. T. W.; Stranks, S. D.; Snaith, H. J.; Nicholas, R. J. Direct Measurement of the Exciton Binding Energy and Effective Masses for Charge Carriers in Organic-Inorganic Tri-Halide Perovskites. *Nat. Phys.* **2015**, *11*, 582−587.
(64) Pathak, A. K.; Prasad, M. D.; Batabyal, S. K. One-Dimensional SbSI Crystals from Sb, S, and I Mixtures in Ethylene Glycol for Solar Energy Harvesting. *Appl. Phys. A: Mater. Sci. Process.* **2019**, *125*, 1−8.
(65) Liu, R.; Mak, C. H.; Han, X.; Tang, Y.; Jia, G.; Cheng, K. C.; Qi, H.; Zou, X.; Zou, G.; Hsu, H. Y. Efficient electronic coupling and heterogeneous charge transport of zero-dimensional Cs4PbBr6 perovskite emitters. *J. Mater. Chem. A* **2020**, *8*, 23803−23811.
(66) Akkerman, Q. A.; Park, S.; Radicchi, E.; Nunzi, F.; Mosconi, E.; De Angelis, F.; Brescia, R.; Rastogi, P.; Prato, M.; Manna, L. Nearly Monodisperse Insulator Cs4PbX6 (X = Cl, Br, I) Nanocrystals, Their Mixed Halide Compositions, and Their Transformation into CsPbX3 Nanocrystals. *Nano Lett.* **2017**, *17*, 1924−1930.
(67) Li, Y.; Shao, W.; Chen, L.; Wang, J.; Nie, J.; Zhang, H.; Zhang, S.; Gao, R.; Ouyang, X.; Ouyang, X.; Xu, Q. Lead-Halide Cs4PbBr6 Single Crystals for High-Sensitivity Radiation Detection. *NPG Asia Mater.* **2021**, *13*, 40.
(68) Di, J.; Li, H.; Su, J.; Yuan, H.; Lin, Z.; Zhao, K.; Chang, J.; Hao, Y. Reveal the Humidity Effect on the Phase Pure CsPbBr3 Single Crystals Formation at Room Temperature and Its Application for Ultrahigh Sensitive X-Ray Detector. *Adv. Sci.* **2022**, *9*, 2103482.
(69) Pawar, E. Related Papers Strength Appraisal of Fibre Reinforced Concrete with Partial Replacement of OPC with Mineral Review Article on Acrylic PMMA. *IOSR J. Mech. Civ. Eng.* **2016**, *13*, 1−4.
(70) Jeedi, V. R.; Narsaiah, E. L.; Yalla, M.; Swarnalatha, R.; Reddy, S. N.; Sadananda Chary, A. Structural and Electrical Studies of PMMA and PVdF Based Blend Polymer Electrolyte. *SN Appl. Sci.* **2020**, *2*, 1−10.
(71) Chen, D.; Wan, Z.; Zhou, Y.; Huang, P.; Ji, Z. Ce3+ Dopants-Induced Spectral Conversion from Green to Red in the Yb/Ho: NaLuF4 Self-Crystallized Nano-Glass-Ceramics. *J. Alloys Compd.* **2016**, *654*, 151−156.
(72) Oliveira, E.; Bértolo, E.; Núñez, C.; Pilla, V.; Santos, H. M.; Fernández-Lodeiro, J.; Fernández-Lodeiro, A.; Djafari, J.; Capelo, J. L.; Lodeiro, C. Green and Red Fluorescent Dyes for Translational


https://doi.org/10.1021/acsomega.2c05862
*ACS Omega* 2023, 8, 4616−4626

Applications in Imaging and Sensing Analytes: A Dual-Color Flag. *ChemistryOpen* **2018**, *7*, 9−52.



https://doi.org/10.1021/acsomega.2c05862
*ACS Omega* 2023, 8, 4616−4626